On the non-conjugacy of nightside aurora and their generator mechanisms

J. P. Reistad,[1,2] N. Østgaard,[1,2] K. M. Laundal,[3] and K. Oksavik[1,2]

Received 28 November 2012; revised 18 April 2013; accepted 24 April 2013.

[1] We have investigated a data set of 19 h of simultaneous global conjugate auroral imaging from space. The data set consists of 10 sequences with durations from 1 to 5 h during active geomagnetic conditions (average $AE \sim 400$ nT). We have identified 15 features (including two presented earlier) of auroral forms that appear mainly in one hemisphere, and we define this as non-conjugate aurora. Three generator mechanisms has been suggested for producing interhemispheric currents and non-conjugate aurora: (1) Hemispherical differences in solar wind dynamo efficiency due to interplanetary magnetic field (IMF) B_x and dipole tilt angle leading to asymmetric region 1 currents in the two polar hemispheres, (2) interhemispheric currents induced by the penetration of IMF B_y into the closed nightside magnetosphere, and (3) hemispheric differences in ionospheric conductivity controlled by the dipole tilt angle inducing interhemispheric currents on closed field-lines. We want to find out if our observations are consistent with these mechanisms. Our analysis shows that five features were consistent with the IMF B_y penetration mechanism, seven features consistent with the solar wind dynamo mechanism, three features consistent with the conductivity mechanism, and two features could not be explained by any of the three suggested mechanisms. Because two features were consistent with two different mechanisms, the numbers add up to 17 although the total number of features is 15. The analysis also shows the expected correlation between the magnitude of the longitudinal shift of conjugate points, ΔMLT, and the occurrence of non-conjugate aurora consistent with the B_y mechanism.

Citation: Reistad, J. P., N. Østgaard, K. M. Laundal, and K. Oksavik (2013), On the non-conjugacy of nightside aurora and their generator mechanisms, *J. Geophys. Res. Space Physics*, *118*, doi:10.1002/jgra.50300.

1. Introduction

[2] Simultaneous imaging of the aurora from both hemispheres offers a unique opportunity to investigate the magnetosphere-ionosphere coupling and how the aurora in the two polar hemispheres responds to varying interplanetary magnetic field (IMF) and solar wind (SW) conditions. Occasionally, simultaneous observations of the aurora in conjugate regions can be made. Ground-based studies, such as *Sato et al*. [1998a, 1998b] and *Motoba et al*. [2011, 2012], have reported both conjugate and non-conjugate features of the aurora, focusing mostly on the hemispheric shifts of conjugate points. Simultaneous aircraft campaigns in the conjugate hemispheres have also been used to obtain optical data to overcome challenges related to cloud cover during auroral display [*Stenbaek-Nielsen and Davis*, 1972; *Stenbaek-Nielsen and Otto*, 1997].

[3] Conjugate imaging from space was first possible in the mid-1980s by Viking and Dynamics Explorer 1. Using these satellites, the first conjugate observations of theta aurora were made [*Craven et al*., 1991]. More than a decade later, conjugate imaging from space was again possible by imagers onboard the IMAGE (Imager for Magnetopause-to-Aurora Global Exploration) and the Polar satellites. From this constellation a number of studies have advanced our understanding of the mechanisms responsible for generating asymmetric aurora either in location [e.g., *Østgaard et al*., 2003, 2011b] or in intensity [*Laundal and Østgaard*, 2009].

[4] Based on earlier findings from conjugate imaging using IMAGE WIC (Wideband Imaging Camera) and Polar VIS (Visible Imaging System) Earth (which is a UV camera), *Østgaard and Laundal* [2012] have suggested that the observed asymmetry can be explained in terms of asymmetric currents. They propose three generator mechanisms producing asymmetric currents in conjugate regions consistent with statistical results and their own findings:

[5] 1. Hemispheric differences in SW dynamo efficiency. By SW dynamo we mean the current generator located in the Earth's bow shock and/or high-latitude magnetopause during IMF B_z negative [*Lopez et al*., 2011; *Guo et al*., 2008; *Siscoe and Siebert*, 2006]. In the following, IMF components will be referred to only by its component, i.e., B_x, B_y, and B_z. The SW flow represents an electric field seen

[1]Department of Physics and Technology, University of Bergen, Bergen, Norway.
[2]Birkeland Centre for Space Science, Bergen, Norway.
[3]Teknova, Kristiansand, Norway.

Corresponding author: J. P. Reistad, Department of Physics and Technology, University of Bergen, P.O. Box 7803, N-5020 Bergen, Norway. (jone.reistad@ift.uib.no)

2169-9380/13/10.1002/jgra.50300

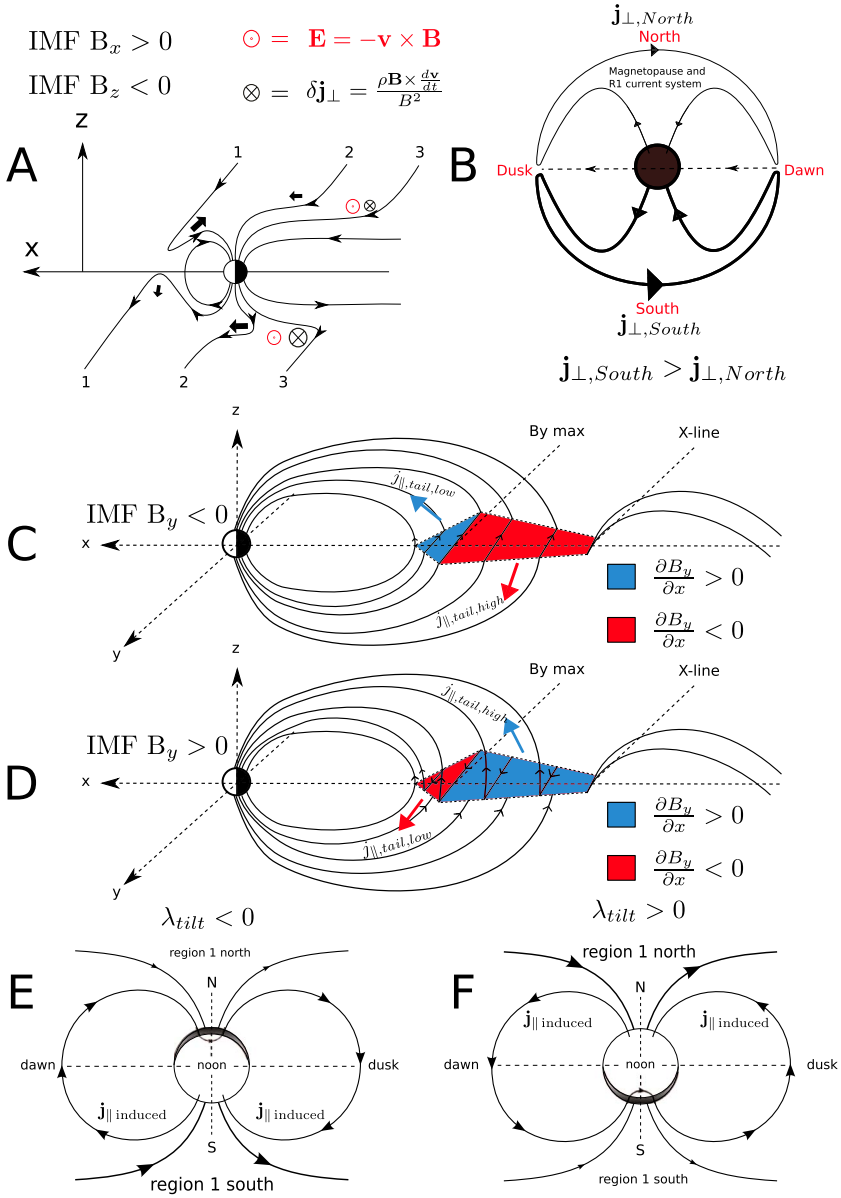

Figure 1. Schematics explaining the three generator mechanisms of non-conjugate aurora. (A) Larger magnetic tension forces in the Southern Hemisphere (black large arrows) than in the Northern Hemisphere on open field-lines on the high-latitude magnetopause in the presence of a positive B_x during negative B_z. Adapted from *Cowley* [1981, Figure 2]. (B) Associated current systems showing larger current in the Southern Hemisphere and possibly brighter aurora. (C) Penetration of B_y into the closed magnetosphere and how the B_y magnitude distributes in the tail during negative B_y conditions. Adapted from *Stenbaek-Nielsen and Otto* [1997, Figure 4]. Associated interhemispheric currents indicated with red and blue arrows. (D) Same as Figure 1C but for B_y positive. (E) Induced interhemispheric currents due to conductivity differences in conjugate regions during negative λ_{tilt}. Adapted from *Benkevich et al.* [2000, Figure 1]. (F) Same as Figure 1E but for positive λ_{tilt}.

in the reference frame of the Earth. For B_z negative conditions, magnetic flux from the dayside is convected across the polar caps resulting in a dawn-dusk electric field. The magnetic tension force (illustrated with black arrows in Figure 1A) decelerates the plasma in the high-latitude magnetosheath tailward of the cusp (field-lines labeled 2 and 3 in Figure 1A), converting kinetic energy from the SW to electromagnetic energy. As a result the existing magnetopause current is believed to increase according to $\delta\mathbf{j}_\perp = \frac{\mathbf{B} \times \rho \frac{d\mathbf{v}}{dt}}{B^2}$, and flow opposite to the SW electric field for the given geometry (i.e., a dynamo, $\delta\mathbf{j} \cdot \mathbf{E} < 0$). *Cowley* [1981] suggested that the presence of a B_x component will favor this effect in one hemisphere. Figure 1A shows a sketch similar to *Cowley* [1981] of how the Northern and Southern Hemisphere magnetic tension forces (black arrows in Figure 1A) on open field-lines differ in the high-latitude magnetosheath (labels 2 and 3 in Figure 1A). The hemispheric difference in magnetic tension due to B_x on the

initially same field-lines (2 and 3) is believed to result in different $\delta \mathbf{j}_{\perp}$ in the two hemispheres. Hence, the SW dynamo is more efficient in one hemisphere, here the Southern Hemisphere. Figure 1B shows the asymmetric currents due to B_x seen from the tail. The expected stronger high-latitude magnetopause current in the Southern Hemisphere are shown with the thicker line, consistent with the B_x positive conditions in Figure 1A. Because the region 1 currents are commonly believed, at least to some extent, to connect to the high-latitude magnetopause current [*Lopez et al*., 2011; *Guo et al*., 2008; *Siscoe and Siebert*, 2006], the field-aligned current strength will be different in the two hemispheres. This might serve as one possible explanation for the hemispheric asymmetries in brightness of the aurora in areas of upward region 1 currents. According to the well-known statistical distribution of the region 1/region 2 current system by *Iijima and Potemra* [1978], this corresponds to a location close to the open-closed field-line boundary from around 12–24 magnetic local time (MLT). Such a B_x effect in the nightside is not well documented in the literature although *Liou et al*. [2001] reported a minor nightside B_x influence on substorm onset location. From Figure 1A it is clear that the dayside is affected by this mechanism, but the nightside effect might work in a different manner. However, in this paper we will attribute non-conjugate features appearing all the way to midnight to this mechanism if the IMF criteria are also satisfied. Further research on this topic is needed to better understand the observed effect, for instance, how far into the nightside this mechanism is important. The dipole tilt angle, λ_{tilt}, when defined as positive toward the Sun in the geocentric solar magnetospheric (GSM) *xz*-plane in the Northern Hemisphere, is believed to enhance this effect for the same sign as B_x. Geometrical considerations suggest that a nonzero λ_{tilt} will result in an effective $\Delta B_x = -B_z \cdot sin(\lambda_{\text{tilt}})$. When B_z is negative, as required for the SW dynamo mechanism to be present, negative (positive) λ_{tilt} will result in a negative (positive) ΔB_x, respectively, making this a secondary contributing factor. From these arguments, brighter aurora is expected in the Northern (Southern) Hemisphere in the 12–24 MLT sector for B_x negative (B_x positive), respectively, when not taking λ_{tilt} into account. Statistical observational results of a B_x asymmetry of the auroral brightness were presented by *Shue et al*. [2002] using the Polar Ultraviolet Imager. Consistent with the presented theory, they found the Northern Hemisphere aurora to be brighter in the premidnight sector for negative B_x compared to positive B_x during B_z negative. They observed the effect to be most prominent during winter conditions, favoring negative λ_{tilt}. Also, the statistical study of *Baker et al*. [2003] supports the correlation between negative B_x and auroral brightness in the Northern Hemisphere.

[6] 2. Penetration of B_y into the closed magnetosphere. By correlating the terrestrial B_y component at geosynchronous orbit [*Wing et al*., 1995] and further downtail in the plasma sheet between 10 and 30 Earth radii [*Lui*, 1984] with IMF B_y it is clear that IMF B_y penetrates into the closed magnetosphere. This validates to some extent the simple theoretical "dipole plus uniform" model predicting the same asymmetric footprints of closed field-lines in the nightside region [*Cowley et al*., 1991]. Motivated by the results of *Lui* [1984] and *Wing et al*. [1995], *Stenbaek-Nielsen and Otto* [1997] presented a sketch indicating how the penetrated B_y is distributed along the *x*-axis in the magnetotail. A reproduction of that figure is shown in Figures 1C and 1D for negative and positive B_y, respectively. The field-aligned terms of Ampéres law assuming Cartesian coordinates in the equatorial plane are given as:

$$j_{\parallel} = \frac{1}{\mu_0}\left(\frac{\partial B_y}{\partial x} - \frac{\partial B_x}{\partial y}\right) \tag{1}$$

[7] For simplicity we ignore the contributions of the second term on the right side ($\partial B_x/\partial y$), which is associated with tail stretching. For the first term, the gradient of the terrestrial B_y field in *x*-direction will induce an interhemispheric current component. For the specific geometry in Figures 1C and 1D, the magnetospheric "twist" requires a North-south (South-north) current at distances between geosynchronous orbit and the X-line for B_y negative (B_y positive), respectively. The asymmetric auroral intensities during flight campaigns in the two hemispheres were consistent with this mechanism [*Stenbaek-Nielsen and Otto*, 1997]. *Liou et al*. [1998] and *Shue et al*. [2001] both found that the Northern Hemisphere auroral power is greater for B_y negative using Polar Ultraviolet Imager data, which is consistent with an interhemispheric current from north to south in agreement with the theory and observations by *Stenbaek-Nielsen and Otto* [1997]. At tail distances closer to Earth, $\partial B_y/\partial x$ points in the opposite direction suggesting oppositely directed currents mapping to lower latitudes. *Vallat et al*. [2005] reported that during a magnetic storm, a strong (10 nA/m^2) North-south field-aligned current component in the equatorial plane around $L = 4.5$ was seen in Cluster data. This is consistent with the theoretical predictions for B_y positive (see Figure 1D), indicating that the predicted current component closer to the Earth also may exist.

[8] 3. Conductivity differences in conjugate regions. To first order, λ_{tilt} quantifies the different exposure of the two hemispheres to solar radiation with respect to magnetic coordinates. *Benkevich et al*. [2000] suggested that for sufficiently large λ_{tilt}, the difference in conductivity in conjugate regions can result in an interhemispheric current on closed field lines from the summer hemisphere to a region close to the terminator in the winter hemisphere where the conductivity gradient is sufficient. This is illustrated in Figures 1E and 1F for negative and positive λ_{tilt}, respectively. *Laundal and Østgaard* [2009] suggested that their observations of completely asymmetric auroras could partly be explained by this mechanism. Also, studies correlating magnetic indices from both hemispheres suggests that these currents exist [*Lyatskaya et al*., 2008, 2009].

[9] Conductivity differences have also been found to affect the global aurora in a more general sense due to different hemispheric impact of solar radiation. *Newell et al*. [1996] found that brighter aurora occurs more often in the winter hemisphere due to the larger acceleration needed to compensate for the lower conductivity. Because we do not claim to have a perfect solution to the different sensitivities of the two cameras, we will not try to compare the total intensity of the two ovals, and will rather discuss the implication of the Newell effect on our results.

[10] Although the conjugate aspect of the aurora has occasionally been investigated, most of our knowledge is based upon observations from only one hemisphere. This leaves conjugate studies of particular interest because it, to some extent, can serve to validate our understanding of the solar wind-magnetosphere-ionosphere coupling.

[11] In this paper, we present new observations of non-conjugate aurora identified from a 19 h data set from IMAGE WIC and Polar VIS Earth cameras. Having simultaneous auroral imaging in both hemispheres, we will determine if the non-conjugate features are consistent with any of the suggested mechanisms. This is the first study using simultaneous conjugate imaging to address this question. Compared to statistical studies we are able to examine both intensity and location. Although there are only 15 identified features, not enough to claim statistical evidence, it represents a significant advance in understanding the appearance of interhemispheric currents.

2. Data and Method

2.1. Conjugate Imaging Data Set

[12] The 19 h conjugate data set consists of 10 sequences of simultaneous imaging in both hemispheres from May 2001 to December 2002. The sequences contain generally disturbed conditions with an average *AE* index $\sim$400 nT. In all sequences, there is one or more substorms.

[13] The IMAGE satellite [*Burch*, 2000] orbits the Earth in a highly elliptical orbit. In the first years of the mission its apogee was over the Northern Hemisphere. We use data from the WIC camera that provide images every 123 s with 10 s integration time. The WIC camera is sensitive to the Lyman-Birge-Hopfield (LBH) band and a few N-lines of the aurora in the UV range (140–190 nm) [*Mende et al*., 2000]. Apsidal precession of the orbit of the Polar satellite [*Acuña et al*., 1995] resulted in an improved coverage of the Southern Hemisphere by the VIS Earth camera, which is most sensitive to the OI line at 130.4 nm with a small contribution from the LBH band [*Frank et al*., 1995; *Frank and Sigwarth*, 2003]. In our data set, the VIS Earth camera had 54 s cadence with an integration time of 32.5 s.

2.2. Feature Selection

2.2.1. Identifying Asymmetric Features

[14] To identify asymmetries in the nightside oval region, we need to compare the images from the two cameras. We start out with raw images corrected for flat-field variations. First we remove counts related to instrumental noise and dayglow emissions leaving only auroral emissions in the images. To be considered a conjugate image pair, we require that the images from the two cameras are within 60 s. This is to eliminate influence from rapid changes during active displays. Also, the asymmetric intensities of the Earth's magnetic field can lead to differences in charged particle losses. However, for the events considered here, the magnetic field strength differs by $< 20\%$ and is therefore not likely to account for a substantial part of the observed asymmetries.

[15] A major challenge when comparing the WIC and VIS Earth images is the different sensitivity. According to Table 2 in *Frey et al*. [2003], modeled atmospheric response to a constant energy flux of precipitating electrons observed from nadir varies with the mean energy of the precipitation for both LBH (WIC) and 130.4 nm (VIS) emissions. The intensity decreases with increasing mean energy for an isotropic Maxwellian distribution when taking atmospheric absorption into account. The mean energy dependence is most significant for the 130.4 nm (VIS) emissions. When it comes to atmospheric absorption, the LBH (WIC) emissions are far more affected than the 130.4 nm (VIS) emissions as also seen in Table 2 in *Frey et al*. [2003]. The LBH emissions are absorbed by O_2, and effects from solar radiation will alter the atmospheric composition possibly leaving the LBH (WIC) emissions less affected by absorption because the scale height of N_2 is more affected by solar radiation than the scale height of O_2. It is clear that a comparison of the intensities from the two cameras with respect to a common magnetospheric source is not straightforward because a constant relation is not likely to exist due to the above mentioned reasons. Here we show observations from five different dates from various seasons. Using a common intensity ratio between the two cameras for a common magnetospheric source for all five dates is therefore not likely to be physically correct. In the present study, we normalize the intensities based on the intensity along a reference magnetic latitude (MLAT) profile. We require the reference MLAT profile to have the same intensity distribution across the oval in both hemispheres, have intensities well above noise levels, and be located outside the identified asymmetric aurora. Using this method we end up having VIS Earth intensities (in kR) ranging from 2–5 times the WIC intensities (in kR) for the five different dates considered. These ratios are also consistent with intensity ratios at substorm onset from the same dates (not shown).

[16] From this established general intensity relation between the hemispheres we can now identify non-conjugate features from plotting the images with the suggested difference in intensity reflected in the color scaling. From manually inspecting the 10 conjugate image sequences by searching for striking asymmetries in conjugate regions, we have identified 13 new features from five different dates showing significant asymmetric auroral intensity in the 18–04 MLT nightside region. Some events have a single asymmetric feature, others have multiple. For each possible feature we perform a "slice-test" to determine the existence of the feature. In the slice-test we make a latitudinal cut through conjugate regions of the feature in both hemispheres and plot the intensities from both cameras as a function of absolute MLAT, $|MLAT|$, using the identified intensity scaling. To be considered an asymmetric feature, we require (when plotting scaled VIS and pure WIC intensities) that the intensity in conjugate regions should be at least twice as large in one hemisphere. Slice-tests for features in Figures 2–6 are provided as further evidence for claiming that the asymmetries are real.

2.2.2. Categorizing Features

[17] To claim that the identified asymmetries are consistent with the three suggested mechanisms, we use the specific criteria listed below.

[18] For the SW dynamo mechanism the non-conjugate feature needs to be at the poleward edge of the auroral oval in the 18–24 MLT sector in the Northern (Southern) Hemisphere during $B_x < -B_z \cdot \sin(\lambda_{tilt})$ ($B_x > -B_z \cdot \sin(\lambda_{tilt})$) and B_z negative, respectively. This is to ensure that the

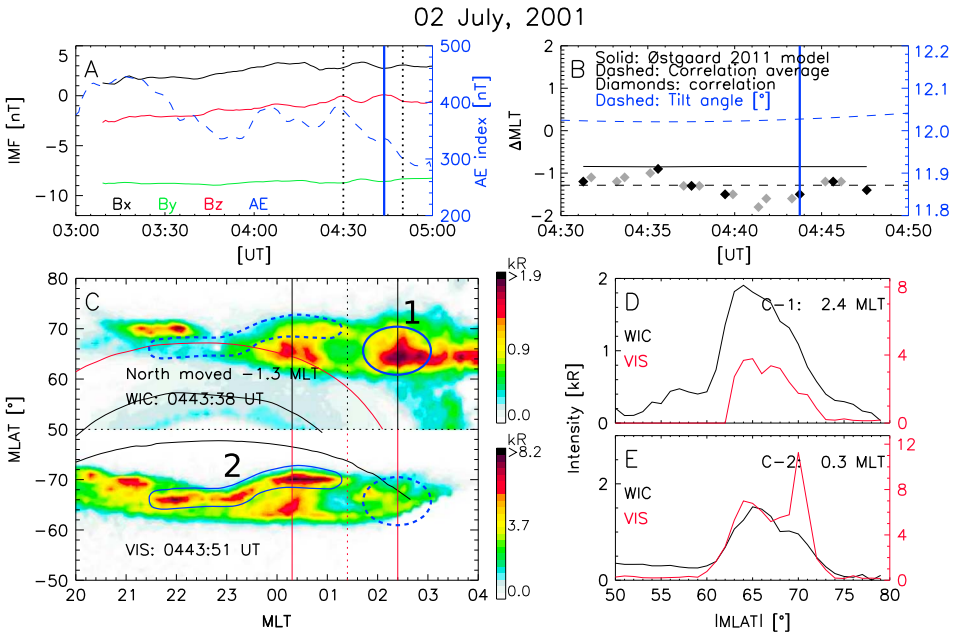

Figure 2. Survey of non-conjugate aurora on 02 July 2001. (A) *AE* index and time-shifted IMF during the event. Vertical dotted lines indicate the time interval of conjugate images in the data set. (B) The hemispheric longitudinal shift, **Δ**MLT, of the aurora as inferred from the image pairs. Diamonds are derived from a 2-D correlation analysis (black is for $\mathbf{r_P > 0.7}$ and overlapping exposure times, grey for $\mathbf{r_P < 0.7}$ and not overlapping exposure times). The solid black line is the expected shift derived from the empirical model by *Østgaard et al.* [2011b] being used as a reference, and the dashed blue line shows λ_{tilt}. The dashed black line is an average of the black diamonds. (C) Nightside plot of conjugate image pair mapped to a rectangular magnetic grid showing the asymmetries 1 and 2. The Northern Hemisphere image is shifted according to the analysis in Figure 2B using the average value (black dashed line). Regions of non-conjugate aurora are indicated with solid blue rings, and the corresponding conjugate area with dashed blue rings. The red line indicates SZA = 100° and the black line SZA = 110°. Location of reference MLAT profile is shown with vertical dashed black/red line. Location of MLAT slices used in the slice-tests in Figures 2D–2E is shown with solid vertical black/red lines in Figure 2C. Slice tests of the asymmetries 1 and 2 (D–E) show MLAT profiles of the intensity from both hemispheres where VIS intensity is scaled according to the reference MLAT profile to allow identification of intensity differences in conjugate regions by comparing the two camera curves. Feature 1 in Figure 2C is consistent with the $\mathbf{B_y}$ and conductivity mechanism and feature 2 in Figure 2C is consistent with the SW dynamo and conductivity mechanism.

SW dynamo is more efficient in the hemisphere observing the bright asymmetry when also λ_{tilt} is taken into account. The 18–24 MLT sector is chosen based on the same arguments as in the introduction section and because we only consider the 18–04 MLT sector in our analysis.

[19] For the B_y mechanism we apply no morning/evening preference for where the non-conjugate aurora should appear. To be considered a B_y effect we require that the non-conjugate aurora must be either on the poleward part of the oval in the Northern (Southern) Hemisphere for B_y negative (B_y positive) or on the equatorward part of the oval in the Northern (Southern) Hemisphere for B_y positive (B_y negative), respectively. Also, the observed longitudinal shift between the hemispheres in the nightside region, ΔMLT, must be in the same direction as expected from the sign of B_y. The latter is to make sure that the IMF B_y has indeed penetrated into the closed magnetosphere.

[20] To be consistent with the conductivity mechanism, we require asymmetric bright aurora to be seen in the summer hemisphere sunlit dawn sector and/or in the winter hemisphere dusk sector close to the terminator consistent with Figures 1E and 1F [*Benkevich et al.*, 2000]. By close to the terminator we mean in a region where solar radiation affects the conductivity along the field line. We require both ends of the field line threading the asymmetry to have a solar zenith angle (SZA) less than 110°. This corresponds to darkness below 400 km altitude.

[21] One should notice that these criteria are more stringent than what has been used in statistical studies [e.g., *Liou et al.*, 1998; *Shue et al.*, 2002] because not only the IMF and λ_{tilt} are considered, but also the predicted location in the nightside sector.

2.3. Interplanetary Magnetic Field Data

[22] We use 1 min IMF and SW data extracted from NASA's Space Physics Data Facility, http://omniweb.gsfc.nasa.gov [e.g., *King and Papitashvili*, 2005]. These data have been time-shifted to the nose of the Earth's bow shock (assumed to be at $x = 17\ R_E$) using the *Weimer et al.* [2003] method. To account for the additional propagation time needed for SW conditions to affect the ionosphere, we further shift the IMF data to a distance of $x = -10\ R_E$ when evaluating the SW dynamo mechanism. This further shift

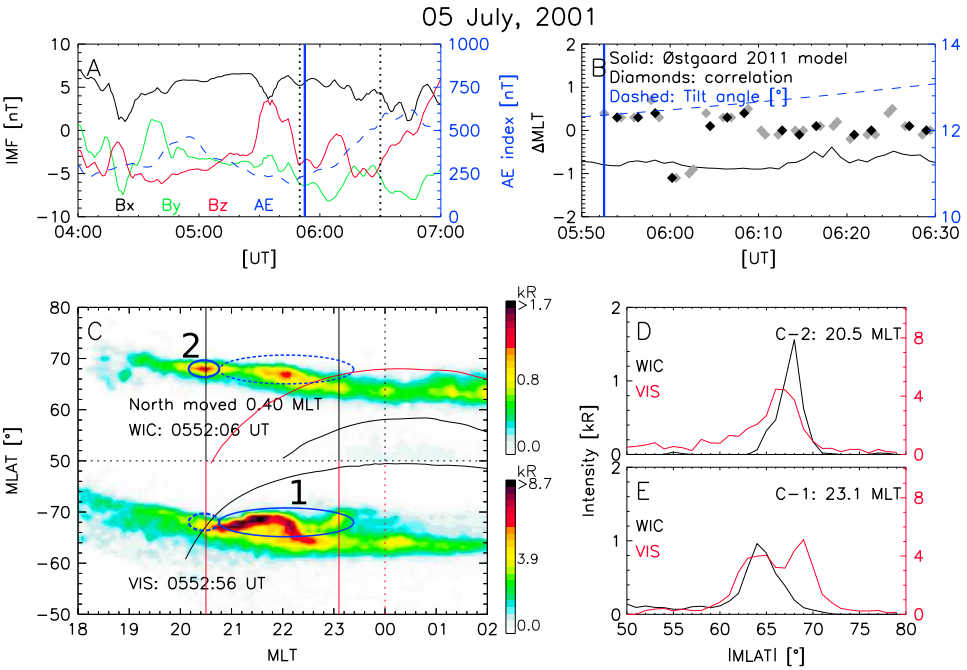

Figure 3. Survey of the non-conjugate aurora event on 05 July 2001. (A–C) The same format as Figure 2A–2C. Feature 1 in Figure 3C is consistent with the SW dynamo mechanism. Feature 2 in Figure 3C is not consistent with any of the three mechanisms. (D–E) Slice-tests of features 2C-2 and 2C-1, respectively.

is based on an average of the present SW velocity. This corresponds to about 5–7 min for SW speeds between 400 and 600 km/s, which is characteristic for our data set. The propagation to $x = -10$ R_E has earlier been used to investigate substorm phenomena [e.g., *Østgaard et al.*, 2004, 2011a] and we believe that for processes on open field-lines like the SW dynamo mechanism, this propagation time is relevant. Using, e.g., −20/30 R_E would add only a few minutes, which means we would have to look at the IMF conditions 2–5 min earlier. This will be discussed as the events are presented. In all IMF panels shown in Figures 2A–6A this time shift and GSM coordinates have been used. For the event on 22 October 2001, shown in Figure 4, OMNI data were not available. Instead we have used SW and IMF data from the Wind spacecraft, located at [33,1,2]R_E in GSM coordinates.

[23] When evaluating events for the B_y candidate the time-shift is done differently. Because this mechanism is believed to act on field-lines already reconnected in the tail, the magnetic field-lines need to convect over the entire polar cap. *Motoba et al.* [2011] did a case study on how B_y affects the displacement of closed field-lines using ground-based all-sky cameras and in situ magnetic field measurements in the tail by Cluster. Their results indicated that the closed field-lines in the magnetospheric tail needed about 52 min to reconfigure after a B_y change reached the magnetopause. This time corresponds well with the drift time across a 3000 km wide polar cap for a convection speed of 1 km/s. Therefore, we add a 52 min time shift from the magnetopause ($x = 10$ R_E) before searching for the B_y-induced effect. When considering the B_y mechanism one should therefore use the B_y value, shown in Figures 2A–6A, ~48 min prior to (to the left of) the solid vertical blue line that indicates the center exposure time of the conjugate images.

2.4. Removing Relative Longitudinal Displacement of the Aurora

[24] As mentioned in the introduction, the x and y component of the IMF can introduce hemispheric displacement of conjugate points [*Cowley et al.*, 1991]. To compare the aurora in true conjugate regions (along the same magnetic field-line), we shift the Northern Hemisphere image in both longitude and latitude so that it aligns with the Southern Hemisphere image as good as possible. This is done using a 2-D correlation method, similar to the method described by *Østgaard et al.* [2011a]. The displacement is expressed as ΔMLT and ΔMLAT, where positive values mean that the northern footpoint is duskward or poleward of the southern footpoint, respectively. Because this conjugate shift is believed to vary with local time [*Cowley et al.*, 1991], we identify the shift only in a limited region on the nightside within 20–04 MLT. In this correlation analysis, the mapped images are first transformed to a rectangular grid having a spatial resolution of 0.1 MLT and 1° MLAT. An $m \times n$ array from the nightside region within 20–04 MLT is extracted from both images and we calculate the linear Pearson correlation coefficient (r_P). For each image pair, we displace the WIC image ± 2 MLT hours in 0.1 h MLT steps and ± 5° MLAT in 1° MLAT steps and calculate r_P at each step to identify the (ΔMLT, ΔMLAT) displacement giving the largest r_P.

[25] As a reference for this observed shift, we also show the predicted longitudinal shift derived statistically from substorm onset locations in both hemispheres [*Østgaard et al.*, 2011b]. This predicted value is shown in Figures 2B–6B as a reference for our observed ΔMLT to determine if IMF B_y has penetrated as predicted. The formula is stated explicitly in equation (2) for IMF $|\mathbf{B}| > 5$ nT

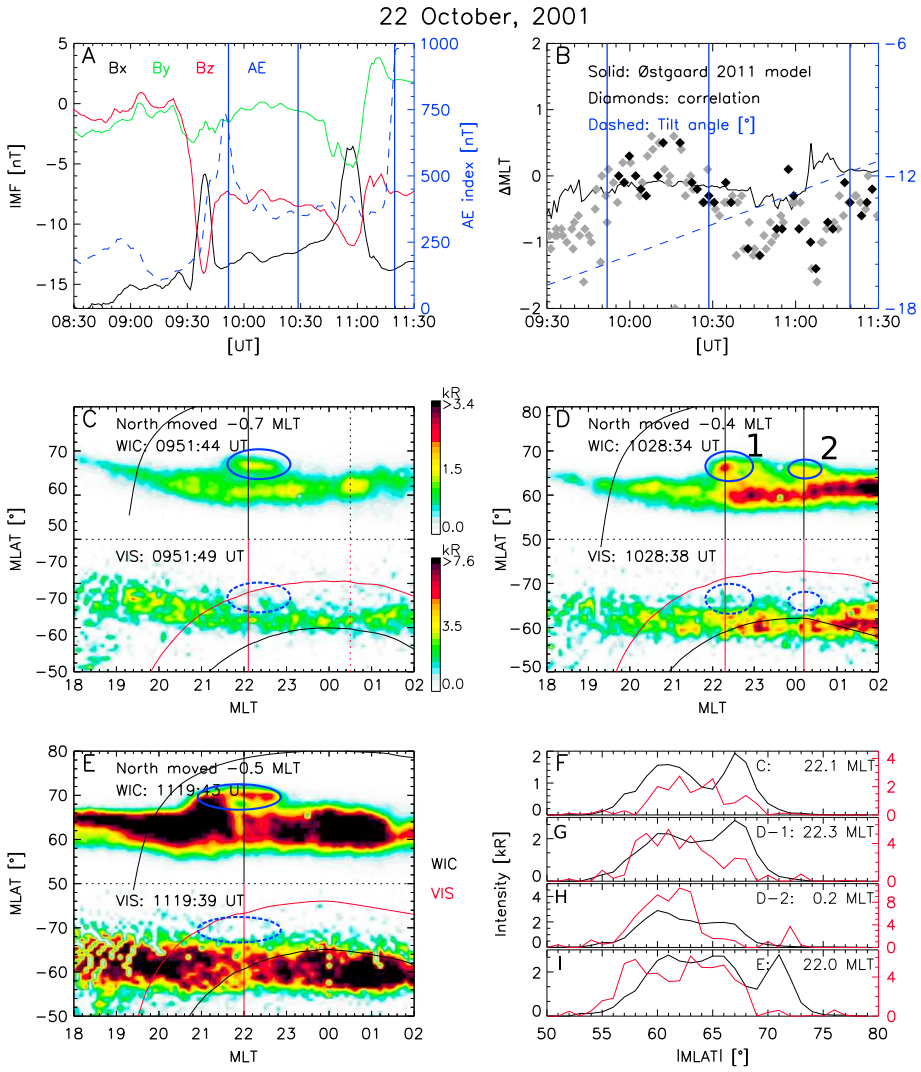

Figure 4. Survey of the non-conjugate aurora event on 22 October 2001. (A and B) The same format as Figure 2A and 2B, respectively. (C–E) The same format as Figure 2C. Slice-tests through the highlighted features are shown in Figure 4F–4I. Features 4C, 4D-1, and 4E is consistent with the SW dynamo and B_y mechanisms and feature 4D-2 is consistent with the B_y mechanism.

as a function of $\theta_c \in [0°, 360°]$. Here θ_c is the IMF clock angle in degrees, defined as the angle between the GSM z-axis and the IMF vector in the yz-plane, positive in the clockwise direction.

$$\Delta\text{MLT} = \text{MLT}_{\text{south}} - \text{MLT}_{\text{north}} = 0.73 \cdot \sin(\theta_c - 4.8°) - 0.17 \quad (2)$$

3. Observations

[26] We have investigated 15 features in the non-conjugate auroral events selected from the 19 h conjugate data set. In this study we have identified 13 new features that will be presented, whereas the two others are from the 12 May 2001 event reported by *Laundal and Østgaard* [2009]. We apply the criteria mentioned in the previous section and categorize the events according to the three generator mechanisms. The following interpretation in terms of the three mechanisms is summarized in Table 1 together with its respective IMF and λ_{tilt} and will be discussed in the next section.

3.1. 02 July 2001 Event

[27] Figure 2 shows one example of asymmetric aurora from the conjugate imaging data set. This event is dominated by a strong negative B_y during negative B_z, a small positive B_x, $\lambda_{\text{tilt}} = 12°$, and a steady SW, meaning that time-shift is not crucial, see Figures 2A and 2B. The time span of conjugate coverage is identified with vertical dotted lines in Figure 2A. A solid vertical blue line in Figures 2A and 2B indicates the center of exposure time of the conjugate image pair shown in Figure 2C.

[28] Figure 2B shows the result of the displacement correlation analysis explained in section 2.4. For each image pair, the displacement (ΔMLT, ΔMLAT) giving the greatest r_P is plotted as diamonds in Figure 2B. The black diamonds are image pairs with overlapping integration times and having $r_P > 0.7$, and the rest of the data are grey diamonds. For this particular event, the values of r_P are mostly between 0.7 and 0.8, meaning that the color difference is only due to

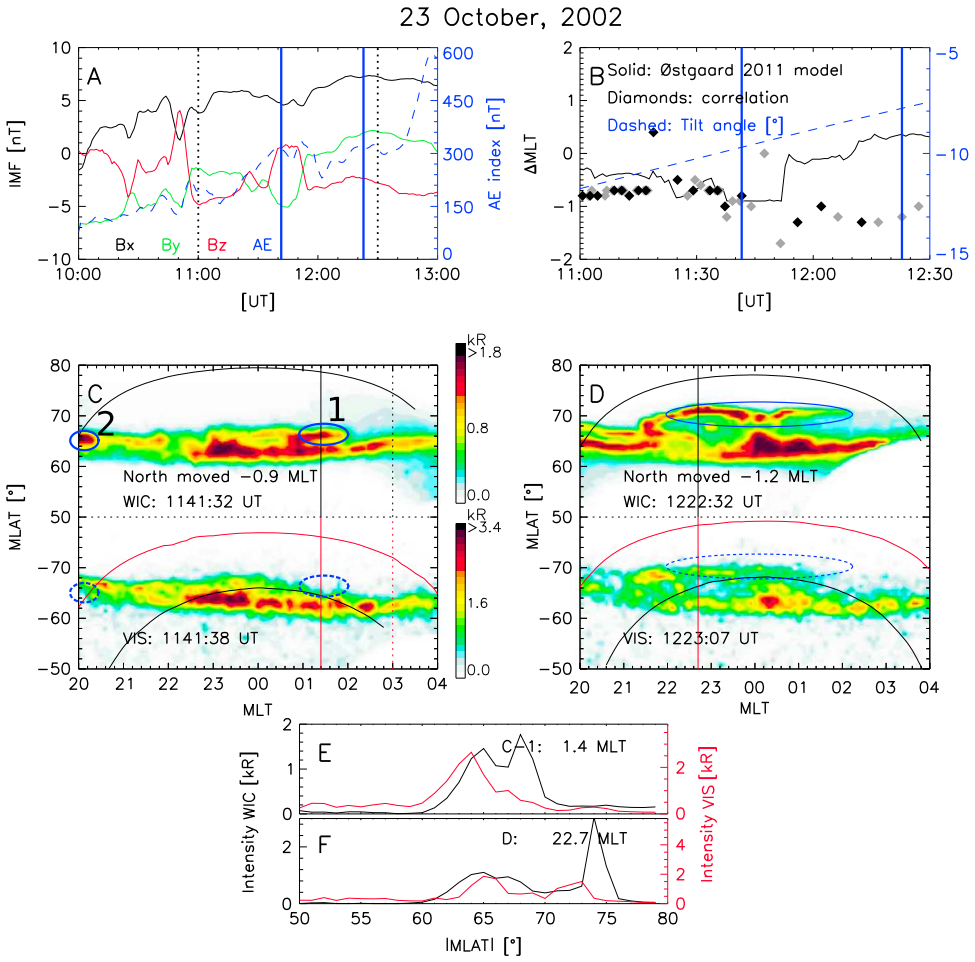

Figure 5. Survey of the non-conjugate event on 23 October 2002. (A and B) The same format as Figure 2A and 2B. (C–D) Observations of non-conjugate aurora in the same format as Figure 2C. The non-conjugate aurora are highlighted by solid blue ellipses. (E–F) Slice-tests of the identified features in the same format as Figures 2D and 2E. Feature 5C-1 is consistent with B_y mechanism, feature 5C-2 is consistent with B_y and conductivity mechanisms. Feature in 5D is consistent with B_y mechanism.

the overlapping integration time criterion. There was little or no displacement in the latitudinal direction, mostly within the pointing accuracy of 1° MLAT and it is therefore not shown here or in any of the other figures. An average of the black diamonds indicated by the dashed black line in Figure 2B is used as a ΔMLT-shift for the image pair shown in Figure 2C. Also, the predicted curve for ΔMLT defined in equation (2) is shown in Figure 2B as a solid black line. This displacement is only dependent on the IMF clock angle and is therefore fairly constant during this event, which is what we also observe (diamonds). We have also shown λ_{tilt} as a dashed blue line indicating only a moderate hemispheric difference in solar radiation between conjugate regions, although the event is close to solstice. In the conjugate image pair presented in Figure 2C contours of equal SZA is plotted. The red line corresponds to SZA = 100° and the black line SZA = 110° representing the position of where the Sun sets at 100 and 400 km altitude, respectively. Between the two lines the conductivity in the summer hemisphere will decrease to a value similar to the winter hemisphere.

[29] In the conjugate image pair shown in Figure 2C an MLAT profile at 1.4 MLT (indicated with vertical dashed black/red line) is used as reference intensity for plotting the images. From the scales on the color-bars we see that VIS intensity is a factor 4 greater than WIC. The same ratio is used when plotting the slice-tests in Figures 2D and 2E making it possible to compare the two lines directly for identification of asymmetries. This is equivalent to plotting pure WIC and scaled VIS intensity in the same coordinate system.

[30] From this event we identify two main asymmetric features labeled 1 and 2 and encircled by a solid blue ring around the non-conjugate feature and dashed blue around its conjugate area, as can be seen in Figure 2C. The correlation analysis confirms that the expected twisted shape of the magnetosphere due to the strong negative B_y is in the same direction as predicted by equation (2). For feature 1, from now referred to as 2C-1, we observe more intense aurora in the Northern Hemisphere in the 02–03 MLT sector. From the slice-test in Figure 2D we can see that the WIC intensity is about twice the scaled VIS intensity. The location of the slice-test is indicated with the solid vertical black/red line at 2.4 MLT in Figure 2C. Because the B_y is negative and

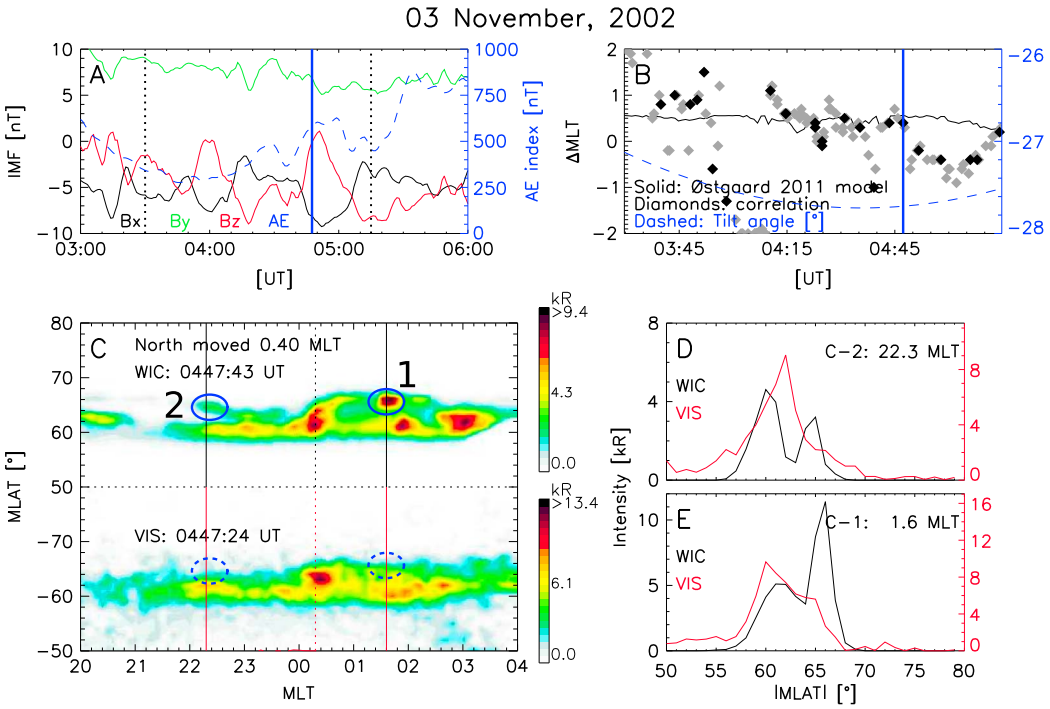

Figure 6. Survey of the non-conjugate event on 03 November 2002. (A and B) The same format as Figures 2A and 2B. (C) Observations of non-conjugate aurora in the same format as Figure 2C. The non-conjugate aurora are highlighted by solid blue ellipses. (E–F) Slice-tests of the identified features in the same format as Figures 2D and 2E. Feature 6C-1 is not consistent with any of the three mechanisms. Feature 6C-2 is consistent with the SW dynamo mechanism.

the location can be considered to be in the poleward segment in the Northern Hemisphere, this observation is consistent with the B_y penetration mechanism. The postmidnight location excludes the SW dynamo mechanism. Because parts of the conjugate area (Southern Hemisphere) have SZA less than 110° and the location is as expected from Figure 1F, the asymmetry is also consistent with the conductivity mechanism.

[31] Feature 2C-2 shows a feature on the poleward edge of the oval in the Southern Hemisphere between 22 and 01 MLT consisting of three bright areas oriented in the longitudinal direction. This is very different from what is observed in the Northern Hemisphere (corresponding blue dashed path). A slice-test along 0.3 MLT is shown in Figure 2E. Here it is clear that the intensity distribution across the oval is different in conjugate regions. The poleward intensity in the Southern Hemisphere is dominant during this event indicating this is not a transient feature. This is consistent with a more efficient SW dynamo in the Southern Hemisphere, which is expected due to the positive B_x and λ_{tilt}. Because the feature exceeds midnight in longitudinal extent it should, strictly speaking, not be associated with the SW dynamo mechanism. However, because this is a dominant feature mainly located premidnight, we include this as a SW dynamo feature in Table 1. Because the B_y is negative and 2C-2 is located mainly at the poleward edge in the Southern Hemisphere, the B_y mechanism is not consistent with the observation. According to the theory by *Benkevich et al.* [2000], a pair of upward and downward field-aligned currents should coexist. As we already have pointed out that feature 2C-1 is consistent with this mechanism, the duskward part of feature 2C-2 might be the manifestation of this opposite directed current. We include this feature with parenthesis around the conductivity mechanism in Table 1 as an alternative explanation because it does not strictly meet the SZA criterion.

3.2. 05 July 2001 Event

[32] Figure 3 shows a survey of the 05 July 2001 event in the same format as Figure 2. IMF conditions shown in Figure 3A show a positive B_x, a negative B_y (of about the same strength), a negative B_z, and $\lambda_{tilt} = 12°$. Using a slightly different time-shift as discussed in section 2.3 would not alter the IMF values significantly for this event. From the image pair in Figure 3C we identify the auroral structure 3C-1 at the poleward boundary of the oval in the Southern Hemisphere. The slice-test shown in Figure 3E at 23.1 MLT indicates a structure in the Southern Hemisphere, which cannot be seen in the Northern Hemisphere. Also, duskward of this feature, the poleward boundary in the Southern Hemisphere seems to be brighter than its Northern Hemisphere counterpart. We show the slice-test from 23.1 MLT rather than in the center of the asymmetry because it is here we see the largest difference in the intensity distribution. Hence, the result is less dependent on the intensity ratio from the reference MLAT profile. Figure 3B shows that λ_{tilt} is positive, which together with the positive B_x indicates that the SW dynamo is more efficient in the Southern Hemisphere. The longitudinal asymmetry identified in Figure 3B is oppositely directed (but small), compared to the output from equation (2) (solid line in same plot). The disagreement between equation (2) and the observed ΔMLT (diamonds) indicates that the IMF B_y has not penetrated the closed magnetosphere as expected.

Table 1. Distribution of the Non-conjugate Events Among the Three Suggested Generator Mechanisms. Parenthesis Is Used When Features Not Strictly, but Almost Matches the Criteria, or if One Mechanism Is Believed to Be Less Important Compared to the Other[a]

	IMF				Generator Mechanism			
Date/Time [UT]	B_x [nT]	B_y [nT]	B_z [nT]	λ_{tilt}	SW Dynamo	B_y	Conductivity	Feature
12 May 2001/21:45	8	0	−3	21°	–	–	+	[a]
12 May 2001/21:45	8	0	−3	21°	+	–	+	[a]
02 July 2001/04:41	3	−8	−2	12°	–	+	+	2C-1
02 July 2001/04:41	3	−8	−2	12°	+	–	(+)	2C-2
05 July 2001/05:53	5	−4	−4	12°	+	–	–	3C-1
(05 July 2001/05:53)	5	−4	−4	12°	–	–	–	(3C-2)
22 October 2001/09:52	−13	−1	−8	−16°	+	(+)	–	4C
22 October 2001/10:29	−13	−2	−8	−14°	+	(+)	–	4D-1
22 October 2001/10:29	−13	−2	−8	−14°	–	+	–	4D-2
22 October 2001/11:20	−14	−1	−7	−12°	+	(+)	–	4E
23 October 2002/11:41	5	−5	0	−10°	–	+	–	5C-1
23 October 2002/11:41	5	−5	0	−10°	–	+	(+)	5C-2
23 October 2002/12:23	7	−4	−4	−7°	–	+	–	5D
03 November 2002/04:48	−8	7	−1	−28°	–	–	–	6C-1
03 November 2002/04:48	−8	7	−1	−28°	+	–	–	6C-2
Total					7(+0)	5(+3)	3(+2)	None: 1(+1)

[a] = [*Laundal and Østgaard*, 2009]

Hence, the B_y candidate cannot explain the asymmetry. An SZA greater than 110° in the Southern Hemisphere also excludes the conductivity mechanism.

[33] A second feature, 3C-2 in the same image pair, is located around 20–21 MLT in the Northern (summer) Hemisphere. From the corresponding slice-test in Figure 3D, the intensity distribution is similar in the two hemispheres and the difference in intensity is close to a factor 2 using the indicated intensity ratio. This feature is included in Table 1 but with parenthesis to emphasize its less distinct nature. The positive B_x excludes the SW dynamo mechanism. The dusk location is not consistent with Figure 1F, hence the conductivity mechanism is also excluded. Finally, the disagreement of equation (2) and observed ΔMLT makes this observation not consistent with any of the three mechanisms.

3.3. 22 October 2001 Event

[34] On 22 October 2001 the conjugate data set covers 5 h from 07 UT until 12 UT. In Figure 4 we present three image pairs showing non-conjugate aurora. Because these observations are separated by ∼40 min we let them count as single events in Table 1. During these observations the IMF was dominated by a strong negative B_x and B_z, and a slightly negative B_y. λ_{tilt} varied from −16° to −12° during the same interval. Using a slightly different time-shift as discussed in section 2.3 would not alter the IMF values significantly for this event. The observations are presented in a similar way to the previous figures. In Figures 4C, 4D, and 4E, bright aurora at the poleward edge of the oval can be seen in the Northern Hemisphere only, in the 20–23 MLT premidnight sector, indicated with solid blue ellipses. Corresponding slice-tests are shown in Figures 4F, 4G, and 4I, respectively, suggesting that the poleward structure in the Northern Hemisphere is not seen in the Southern Hemisphere. Because B_x, B_z, and λ_{tilt} are all negative as seen in Figures 4A and 4B, we attribute this asymmetry to the SW dynamo mechanism. When using the +48 min time-shift, B_y is also slightly negative during all these observations, making the B_y mechanism also a possible candidate, but not likely. We believe that the SW dynamo candidate is the most important mechanism because the IMF is dominated by a large negative B_x (∼ − 12 nT), and the longitudinal shift ΔMLT only occasionally reaches values larger than 1 h. For most of the time it fluctuates close to 0, as can be seen in Figure 4B. To indicate the suggested minor importance of the B_y mechanism, we put parentheses around this mechanism in Table 1.

[35] In Figure 4D a second feature, 4D-2, is highlighted. The corresponding slice-test is shown in Figure 4H. Again, the Northern Hemisphere aurora is brighter on the poleward edge, here by a factor of 2 using the indicated scaling. In the main part of the oval the intensity is greater in the Southern Hemisphere, also by a factor 2. This is a minor asymmetry compared to the rest of the features from this day, but is included in Table 1 because it passes the slice-test. The prevailing conditions are only consistent with the B_y mechanism for this feature. For all features presented in Figure 4, the winter hemisphere SZA is larger than 110° excluding the conductivity mechanism.

3.4. 23 October 2002 Event

[36] Two image pairs showing non-conjugate aurora on 23 October 2002 are presented in Figures 5C and 5D. Figure 5A shows southward IMF where the radial components are about equal where B_x is positive and B_y is negative. Using a slightly different time-shift as discussed in section 2.3 would not alter the IMF values significantly for this event. Figure 5B shows that ΔMLT is indeed as expected due to penetration of IMF B_y. A reference MLAT profile is used at 03 MLT. Here the intensity distribution across the oval is similar and believed to be outside the regions of non-conjugate aurora. In Figure 5C, a poleward structure is seen in the Northern Hemisphere from 00 to 02 MLT (most intense from 01 to 02 MLT), identified as feature 5C-1. This feature cannot be seen in the Southern Hemisphere as is evident from the corresponding slice-test in Figure 5E. In addition, a bright structure in the Northern Hemisphere at 20 MLT, identified as feature 5C-2, is found to be non-conjugate. We do not show any slice-test of this feature as the color difference is very apparent. Because the asymmetries occur during positive B_x in the Northern Hemisphere, the SW dynamo mechanism is not consistent with our observations. The negative B_y, the poleward

location in the Northern Hemisphere, and the observed $\Delta MLT = -0.9$ allows both feature 5C-1 and 5C-2 to be explained the B_y mechanism. Feature 5C-1 is located far from the 110° SZA line and has a location not consistent with Figure 1E excluding the conductivity mechanism. Feature 5C-2 has a SZA $\gtrsim 110°$ and a location consistent with Figure 1E. We therefore put parenthesis around the conductivity mechanism for this feature in Table 1 to indicate a possible alternative explanation.

[37] In Figure 5D, a similar but more distinct structure is again visible in the Northern Hemisphere from 22 to 02 MLT (solid blue ellipse). Again, the IMF is southward, having a positive B_x and negative B_y (using Figure 5A-48 min). A slice-test at 22.7 MLT (Figure 5 F) indicates an asymmetric intensity distribution for this feature. A much larger intensity with respect to the main oval is observed in the Northern Hemisphere. Because B_x is positive during the whole event and the non-conjugate aurora is observed in the Northern Hemisphere and into the postmidnight sector, the SW dynamo mechanism is not consistent with this observation. The winter hemisphere location has an SZA greater than 110° and hence the conductivity candidate is rejected. From Figure 5B we can see that the observed longitudinal shift is fairly large (−1.2 h), indicating a twisted shape of the magnetosphere due to the negative B_y seen in Figure 5A. Because this feature is located in the Northern Hemisphere at the poleward part of the oval, this observation is consistent with the B_y mechanism.

3.5. 03 November 2002 Event

[38] Our last observation of non-conjugate aurora is shown in Figure 6 and is presented in the same format as Figure 2. The event is dominated by a large $\lambda_{tilt} = -28°$ leaving the whole Southern Hemisphere oval in direct sunlight. The IMF has a steady positive B_y (8 nT) during southward B_z. B_x component is negative and fluctuating. It reaches a value of −8 nT at the time of the conjugate image pair. Using a slightly different time-shift as discussed in section 2.3 would not alter the IMF values significantly for this event. We see in the Northern Hemisphere at 01–02 MLT on the poleward edge of the oval a rather small but very bright spot (solid blue ellipse) that is not present in the Southern Hemisphere. The slice-test in Figure 6E confirms that the spot is very bright compared to the aurora in the conjugate region. Although B_x is negative, the postmidnight location of the asymmetry excludes the SW dynamo candidate. Because the asymmetry is located on the poleward part of the oval in the Northern Hemisphere during positive B_y, the B_y mechanism is not consistent with the observation. Because $\lambda_{tilt} = -28°$ the asymmetry is far from the terminator in the winter hemisphere (110° SZA line outside the plot in WIC image). Feature 6C-1 is therefore not consistent with the conductivity mechanism, leaving this observation without any explanation mechanism among the three. A less prominent asymmetric feature, 6C-2, is a poleward arc in the Northern Hemisphere that cannot be seen in the Southern Hemisphere. The slice-test in Figure 6D indicates a broad oval in the Southern Hemisphere while a double oval is seen in the Northern Hemisphere. For the same reasons as for feature 6C-1 the B_y and conductivity mechanisms are not consistent with the observation. However, the premidnight location and negative B_x and λ_{tilt} is consistent with the SW dynamo mechanism.

[39] Also, a feature around 03 MLT in the Northern Hemisphere (not highlighted in Figure 6C) appears asymmetric. We find it likely that the ΔMLT shift should be slightly different (close to zero) in this region resulting in only a minor asymmetry. For this event, the Southern Hemisphere oval is directly exposed to sunlight (SZA = 100° line barely touches −50° MLAT in Figure 6C). This might lead to additional uncertainties related to dayglow removal making it difficult to determine the significance of small asymmetries.

4. Discussion

[40] The features presented in Figures 2–6 show that non-conjugate aurora is a fairly common phenomenon because 15 features of large-scale asymmetries are found in the 19 h data set. The observations are categorized in Table 1 by generator mechanism. λ_{tilt} and time-shifted IMF for each event are shown for each feature in separate columns. From the 15 features summarized in the table, any statistical argument on occurrence of the different mechanisms must be considered with great care. We can see that the SW dynamo and B_y features appear almost equally frequent, having 7 and 5 occurrences (not considering the parenthesis features), respectively. For the conductivity mechanism we found 3(+2) consistent features. Two features could not be explained by any of the three suggested mechanisms. The reason why these numbers adds up to more than 15 is that some features are consistent with multiple mechanisms as can be seen in Table 1. Among the two features not consistent with any mechanism, feature 6C-1 shows the largest intensity asymmetry. This is also the event having the largest seasonal difference among all the 15 features. Because the non-conjugate aurora is located in the winter hemisphere, an explanation similar to what was suggested by *Newell et al*. [1996] could possibly account for the observed asymmetry. This is however not the case for the last feature without any matching generator mechanism, feature 3C-2. As mentioned in the observation section, this is a minor asymmetry because it strictly speaking does not match the criterion of a factor 2 in intensity difference as can be seen in Figure 3D. Also, a slightly different time-shift would alter the conclusion, making this a less prominent feature as indicated by its parenthesis in Table 1.

[41] Based on the analysis summarized in Table 1 we claim that non-conjugate auroral features observed in the nightside region are consistent with the three suggested generator mechanisms. By having simultaneous conjugate coverage we have shown that the explained features indeed have the suggested opposite behavior in the two hemispheres as expected. Although there are only small amounts of simultaneous conjugate imaging data available, and the different nature of the two cameras makes it difficult to compare intensities, we have tried to make the selection as objective as possible. However, conclusions on relative strength of the mechanisms cannot be made at this point, but identification and more knowledge about the mechanisms will be of great value for further investigation of non-conjugate aurora. If the suggested generator mechanisms are as important as this study indicates, statistical studies from each hemisphere separately should support these results and give further information of the relative strength and importance of the mechanisms.

[42] From the eight different conjugate image pairs presented in Figures 2–6 we notice a relation between the magnitude of the longitudinal shift, |ΔMLT|, and whether there is a B_y consistent asymmetry. ΔMLT serves as an indicator of how much IMF B_y has penetrated the closed magnetosphere. The associated interhemispheric currents should therefore depend upon the observed ΔMLT. This is in fact what we observe. From the eight different conjugate image pairs presented, four have features consistent with the B_y mechanism. The mean absolute longitudinal shift, $\left|\overline{\Delta \mathrm{MLT}}\right|$, for those events are 1.0 h while for the four events not consistent with the B_y mechanism, $\left|\overline{\Delta \mathrm{MLT}}\right| = 0.5$ h.

[43] B_x control of the aurora has been reported earlier, but only from one hemisphere when using global imaging. *Shue et al*. [2002] and *Baker et al*. [2003] found statistically that the Northern Hemisphere oval is brighter during negative B_x compared to positive B_x. Our results are consistent with their observations and show, for the first time, multiple simultaneous observations from both hemispheres indicating the suggested simultaneous opposite behavior in the two hemispheres, consistent with the expected poleward location.

[44] For all the SW dynamo events, λ_{tilt} has the same sign as B_x. Recall that positive (negative) B_x is believed to mostly affect the Southern (Northern) Hemisphere and λ_{tilt} is defined in a way that a positive (negative) value implies winter conditions in the Southern (Northern) Hemisphere, respectively. Earlier studies [e.g., *Newell et al*., 1996] found that the hemispheric conductivity difference induced by large λ_{tilt} gives brighter aurora in the winter hemisphere as a consequence of enhanced acceleration due to low conductivity. Our observations indicate the expected positive correlation of B_x and λ_{tilt} with SW dynamo efficiency. A consequence of this correlation is that the SW dynamo asymmetry prefers to occur in the winter hemisphere. Influence of the seasonal variations described by *Newell et al*. [1996] is therefore expected in the SW dynamo observations. In fact, all of the SW dynamo observations in this study originate from the winter hemisphere. However, in most of the features attributed to the SW dynamo mechanism, both the region of non-conjugate aurora and its conjugate region would not be in direct sunlight at a height of 130 km, as can be seen in the 22 October 2001 event in Figure 4 by that the features have SZA greater than 100° (red line). The events presented in Figures 2 and 3 have features attributed to the SW dynamo mechanism where the conjugate region have SZA between 90° and 100° making them potentially more influenced by the *Newell et al*. [1996] explanation. This is also true for the B_y feature shown in Figure 5C-2. However, the opposite case is also observed in the data set, meaning non-conjugate aurora in the summer hemisphere as can be seen in features 2C-1 and 3C-2. One should remember that the method used for normalizing the intensities for plotting might remove signatures of mechanisms affecting the general intensity [e.g., *Newell et al*., 1996].

5. Conclusion

[45] We have shown 13 features (plus two from *Laundal and Østgaard* [2009]) of non-conjugate aurora from a 19 h data set of simultaneous imaging of both auroral ovals. This indicates that non-conjugate large-scale (> 300 km) structures of the aurora is a common phenomenon often seen near the poleward boundary of the oval. By categorizing the observations into the three suggested generator mechanisms, we have shown that 13 of 15 features are consistent with these mechanisms. This provides further evidence for the importance of the suggested mechanisms. The suggested SW dynamo control of non-conjugate aurora are consistent with earlier findings from one hemisphere as presented by *Shue et al*. [2002] and *Baker et al*. [2003], but here is shown, for the first time, multiple simultaneous observations from both hemispheres supporting their results. The observations also support the expected correlation between the B_y asymmetry and hemispheric longitudinal shift, ΔMLT.

[46] **Acknowledgments.** The authors thank L. A. Frank for the use of Polar VIS Earth data. We also thank S. B. Mende and the IMAGE FUV team for the use of IMAGE FUV data. We acknowledge the use of NASA/GSFC's Space Physics Data Facility for OMNI data. Also thanks to A. Szabo for the Wind magnetic field data. We thank the Research Council of Norway for financial support.

[47] Robert Lysak thanks the reviewers for their assistance in evaluating this paper.

References

Acuña, M. H., K. W. Ogilvie, D. N. Baker, S. A. Curtis, D. H. Fairfield, and W. H. Mish (1995), The global geospace science program and its investigations, *Space Sci. Rev.*, *71*, 5–21.

Baker, J. B., A. J. Ridley, V. O. Papitashvili, and C. R. Clauer (2003), The dependence of winter aurora on interplanetary parameters, *J. Geophys. Res.*, *108*(A4), 8009, doi:10.1029/2002JA009352.

Benkevich, L., W. Lyatsky, and L. L. Cogger (2000), Field-aligned currents between conjugate hemispheres, *J. Geophys. Res.*, *105*(A12), 27,727–27,737, doi:10.1029/2000JA900095.

Burch, J. L. (2000), Image mission overview, *Space Sci. Rev.*, *91*, 1–14.

Cowley, S. W. H. (1981), Asymmetry effects associated with the x-component of the IMF in a magnetically open magnetosphere, *Planet. Space Sci.*, *29*(8), 809–818.

Cowley, S. W. H., J. P. Morelli, and M. Lockwood (1991), Dependence of convective flows and particle precipitation in the high-latitude dayside ionosphere on the X and Y components of the interplanetary magnetic field, *J. Geophys. Res.*, *96*(A4), 5557–5564.

Craven, J. D., J. S. Murphree, L. A. Frank, and L. L. Cogger (1991), Simultaneous optical observations of transpolar arcs in the two polar caps, *Geophys. Res. Lett.*, *18*(12), 2297–2300.

Frank, L. A., and J. B. Sigwarth (2003), Simultaneous images of the northern and southern auroras from the Polar spacecraft: An auroral substorm, *J. Geophys. Res.*, *108*(A4), 8015, doi:10.1029/2002JA009356.

Frank, L. A., J. B. Sigwarth, J. D. Craven, J. P. Cravens, J. S. Dolan, M. R. Dvorsky, P. K. Hardebeck, J. D. Harvey, and D. W. Muller (1995), The visible imaging system (VIS) for the Polar Spacecraft, *Space Sci. Rev.*, *71*, 297–328.

Frey, H. U., et al. (2003), Summary of quantitative interpretation of IMAGE far ultraviolet auroral data, *Space Sci. Rev.*, *109*(1–4), 255–283, doi:10.1023/B:SPAC.0000007521.39348.a5.

Guo, X. C., C. Wang, Y. Q. Hu, and J. R. Kan (2008), Bow shock contributions to region 1 field-aligned current: A new result from global MHD simulations, *Geophys. Res. Lett.*, *35*, L03108, doi:10.1029/2007GL032713.

Iijima, T., and T. A. Potemra (1978), Large-scale characteristics of field-aligned currents associated with substorms, *J. Geophys. Res.*, *83*(A2), 599–615, doi:10.1029/JA083iA02p00599.

King, J. H., and N. E. Papitashvili (2005), Solar wind spatial scales in and comparisons of hourly Wind and ACE plasma and magnetic field data, *J. Geophys. Res.*, *110*, A02104, doi:10.1029/2004JA010649.

Laundal, K. M., and N. Østgaard (2009), Asymmetric auroral intensities in the Earth's Northern and Southern hemispheres, *Nature*, *460*(7254), 491–493, doi:10.1038/nature08154.

Liou, K., P. T. Newell, C. I. Meng, M. Brittnacher, and G. Parks (1998), Characteristics of the solar wind controlled auroral emissions, *J. Geophys. Res.*, *103*, 17, 543–17,557.

Liou, K., P. T. Newell, D. G. Sibeck, and C.-I. Meng (2001), Observation of IMF and seasonal effects in the location of auroral substorm onset, *J. Geophys. Res.*, 103, 17,543–17,557.

Lopez, R. E., V. G. Merkin, and J. G. Lyon (2011), The role of the bow shock in solar wind-magnetosphere coupling, *Ann. Geophys.*, *29*(6), 1129–1135, doi:10.5194/angeo-29-1129-2011.

Lui, A. T. Y. (1984), Characteristics of the cross-tail current in the Earth's magnetotail, in *Magnetospheric Currents, Geophys. Monogr. Ser*., vol. 1, edited by T. A. Poterma, pp. 158–170, AGU, Washington, D. C.

Lyatskaya, S., W. Lyatsky, and G. V. Khazanov (2008), Relationship between substorm activity and magnetic disturbances in two polar caps, *Geophys. Res. Lett.*, *35*, L20104, doi:10.1029/2008GL035187.

Lyatskaya, S., W. Lyatsky, and G. V. Khazanov (2009), Auroral electrojet AL index and polar magnetic disturbances in two hemispheres, *J. Geophys. Res.*, *114*, A06212, doi:10.1029/2009JA014100.

Mende, S. B., et al. (2000), Far ultraviolet imaging from the IMAGE spacecraft. 2. Wideband FUV imaging, *Space Sci. Rev.*, *91*, 271–285.

Motoba, T., K. Hosokawa, Y. Ogawa, N. Sato, A. Kadokura, S. C. Buchert, and H. Rème (2011), In situ evidence for interplanetary magnetic field induced tail twisting associated with relative displacement of conjugate auroral features, *J. Geophys. Res.*, *116*, A04209, doi:10.1029/2010JA016206.

Motoba, T., K. Hosokawa, A. Kadokura, and N. Sato (2012), Magnetic conjugacy of northern and southern auroral beads, *Geophys. Res. Lett.*, *39*, L08108, doi:10.1029/2012GL051599.

Newell, P. T., C.-I. Meng, and K. M. Lyons (1996), Suppression of discrete aurorae by sunlight, *Nature*, *381*(6585), 766–767, doi:10.1038/381766a0.

Østgaard, N., and K. M. Laundal (2012), Auroral asymmetries in the conjugate hemispheres and interhemispheric currents, in *Auroral Phenomenology and Magnetospheric Processes: Earth and Other Planets, Geophys. Monogr. Ser*., vol. 197, edited by A. Keiling et al., pp. 99–111, AGU, Washington, D. C., doi:10.1029/2011GM001190.

Østgaard, N., S. B. Mende, H. U. Frey, L. A. Frank, and J. B. Sigwarth (2003), Observations of non-conjugate theta aurora, *Geophys. Res. Lett.*, *30*(21), 2125, doi:10.1029/2003GL017914.

Østgaard, N., S. B. Mende, H. U. Frey, and T. J. Immel (2004), Interplanetary magnetic field control of the location of substorm onset and auroral features in the conjugate hemispheres, *J. Geophys. Res.*, *109*, A07204, doi:10.1029/2003JA010370.

Østgaard, N., B. K. Humberset, and K. M. Laundal (2011a), Evolution of auroral asymmetries in the conjugate hemispheres during two substorms, *Geophys. Res. Lett.*, *38*, L03101, doi:10.1029/2010GL046057.

Østgaard, N., K. M. Laundal, L. Juusola, A. Åsnes, S. E. Håland, and J. M. Weygand (2011b), Interhemispherical asymmetry of substorm onset locations and the interplanetary magnetic field, *Geophys. Res. Lett.*, *38*, L08104, doi:10.1029/2011GL046767.

Sato, N., M. Morooka, K. Minatoya, and T. Saemundsson (1998a), Nonconjugacy of pulsating auroral patches near L = 6, *Geophys. Res. Lett.*, *25*(20), 3755–3758.

Sato, N., T. Nagaoka, K. Hashimoto, and T. Saemundsson (1998b), Conjugacy of isolated auroral arcs and non-conjugate auroral breakups, *J. Geophys. Res.*, *103*(A6), 11,641–11,652, doi:10.1029/98JA00461.

Shue, J.-H., P. T. Newell, K. Liou, and C.-I. Meng (2001), Influence of interplanetary magnetic field on global auroral patterns, *J. Geophys. Res.*, *106*(A4), 5913–5926.

Shue, J.-H., P. T. Newell, K. Liou, C. Meng, and S. W. H. Cowley (2002), Interplanetary magnetic field Bx asymmetry effect on auroral brightness, *J. Geophys. Res.*, *107*(A8), 1197, doi:10.1029/2001JA000229.

Siscoe, G., and K. Siebert (2006), Bimodal nature of solar wind-magnetosphere-ionosphere-thermosphere coupling, *J. Atmos. Sol. Terr. Phys.*, *68*(8), 911–920, doi:10.1016/j.jastp.2005.11.012.

Stenbaek-Nielsen, H. C., and T. N. Davis (1972), Relative motions of auroral conjugate points during substorms, *J. Geophys. Res.*, *77*(10), 1844–1858.

Stenbaek-Nielsen, H. C., and A. Otto (1997), Conjugate auroras and the interplanetary magnetic field, *J. Geophys. Res.*, *102*(A2), 2223–2232.

Vallat, C., et al. (2005), First current density measurements in the ring current region using simultaneous multi-spacecraft CLUSTER-FGM data, *Ann. Geophys.*, *23*(5), 1849–1865, doi:10.5194/angeo-23-1849-2005.

Weimer, D. R., D. M. Ober, N. C. Maynard, M. R. Collier, D. J. McComas, N. F. Ness, C. W. Smith, and J. Watermann (2003), Predicting interplanetary magnetic field (IMF) propagation delay times using the minimum variance technique, *J. Geophys. Res.*, *108*(A1), 1026, doi:10.1029/2002JA009405.

Wing, S., P. T. Newell, D. G. Sibeck, and K. B. Baker (1995), A large statistical study of the entry of interplanetary magnetic field Y-component into the magnetosphere, *Geophys. Res. Lett.*, *22*(16), 2083–2086.